Numerical Studies of the Flow Field in a Low Power DC Arcjet Thruster Using Navier-Stokes Equations

Hiroyuki OKAMOTO and Michio NISHIDA
Department of Aeronautical Engineering
Kyushu University
Fukuoka 812, Japan

Ken-ichi TANAKA
Central Research Laboratory
Mitsubishi Electric Corporation
Hyougo 661, Japan

Abstract

Numerical simulation of a low power DC arcjet thruster was performed, using the same nozzle geometry as used in laboratory experiments. The governing equations for propellant gas flows consist of the axisymmetric Navier-Stokes equations coupled with electric field equations. The propellant flow equations were solved by time dependent technique using the TVD-MacCormack scheme. The radiation cooling condition was imposed as the wall condition. Argon was used as propellant. It was considered that the flow was followed by nonequilibrium ionization-recombination. From numerical data, the detail of thruster flow field heated by Joule heating was revealed, and the viscous effects, such as the boundary layer and heat transfer, were discussed.

1. Introduction

Arcjet thrusters have attracted much interest as one of the available propulsion-systems for North-South station keeping of future spacecrafts. In order to predict the performance characteristics of the arcjet thruster, the detail of the flow field interacting with arc currents inside the thruster is required. However, it is actually difficult to directly observe the discharge section. Therefore, we have applied computational simulation to the investigation of the thruster flow field. The computational simulation has an advantage of easily varying parameters such as thruster geometry, arc currents and other conditions.

Computational simulations of the flow field inside arcjet thrusters have been conducted.[1-5] Ao and Fujiwara[1] did a pioneering numerical study of an axisymmetric MPD arcjet thruster by using the MacCormack scheme. Their thruster model was very simple which consisted of a cylindrical bluff-nosed cathode and hollow anode. In their computation, equilibrium ionization-recombination was considered. The numerical study in Ref.2 was the extension of the work in Ref.1, in which the cathode geometry was changed to a pointed cathode. Chanty and Martinez-Sanchez[3] carried out the numerical simulation of an axisymmetric MPD arcjet thruster by a finite volume scheme and included the effect of hall current into the computation. However, it was assumed that electrical conductivities were constant in the entire flow region. Auweter-Kurtz *et al.*[4] also did the numerical simulation of an MPD thruster. In the above four numerical simulations, a Mach number at the thruster inlet was assumed to be supersonic. However, it is reasonable to consider that in an actual thrusters, the flow at the inlet is subsonic.

In a previous study[5], we applied the Euler equations to simulate the flow in the arcjet thruster, so that a boundary layer and hence the heat transfer on the thruster nozzle wall were not considered. However an actual arcjet thruster which will operate in space is radiation-cooled. Therefore, we have to consider the balance of the heat transferred to the wall with irradiated energy from the wall. For this reason, we need to employ the Navier-Stokes equations as the governing equations. Thus, in the present study, numerical simulation of a low power DC arcjet thruster, which has the same geometry as used in laboratory experiments[6], was performed using the Navier-Stokes equations.

2. Governing Equations for Propellant Gas Flows

2.1.Flow Model

Numerical calculations are conducted for the arcjet thruster shown in Fig.1. The flow field treated here is inside the thruster and following assumptions are introduced for the propellant flow computations:

(1) The flow is axisymmetric.
(2) Argon gas considered as propellant. The propellant gas is singly ionized and it is composed of neutral argon atoms, singly ionized ions, and electrons.
(3) The velocities of all species are in equilibrium.
(4) The temperatures are also in equilibrium.
(5) An inflow to the thruster is subsonic and flow at the nozzle exit is supersonic.

(6) Ionization-recombination takes place due to neutral atoms-electron collisions, i.e. the following reaction is considered here:

$$A + e^- = A^+ + e^- + e^-$$

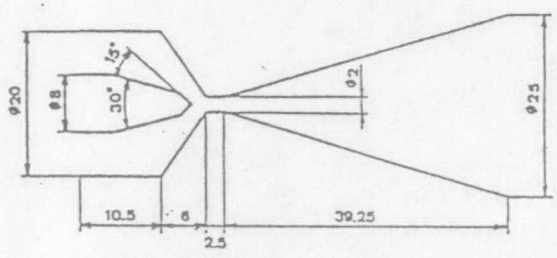

Fig.1 Thruster geometry.

2.2 Governing Equations

The propellant flow equations are numerically solved by a time-dependent method and steady state solutions are obtained as asymptotic solutions for large time steps. Using cylindrical coordinates, the unsteady conservation equations are written as, under the above assumptions,

$$\frac{\partial \boldsymbol{W}}{\partial t} + \frac{\partial \boldsymbol{F}}{\partial z} + \frac{\partial \boldsymbol{G}}{\partial r} + \frac{\boldsymbol{G}}{r} + \frac{\boldsymbol{H}}{r} = \boldsymbol{S} \tag{1}$$

$$\boldsymbol{W} = \begin{bmatrix} \rho \\ \rho u \\ \rho v \\ \rho e \\ n_e \end{bmatrix}, \boldsymbol{F} = \begin{bmatrix} \rho u \\ \rho u^2 - \sigma_{zz} \\ \rho uv - \tau_{rz} \\ \rho ue + \dot{q}_z - \sigma_{zz}u - \tau_{zr}v \\ n_e u \end{bmatrix},$$

$$\boldsymbol{G} = \begin{bmatrix} \rho v \\ \rho uv - \tau_{rz} \\ \rho v^2 - \sigma_{rr} \\ \rho ve + \dot{q}_r - \tau_{zr}u - \sigma_{rr}v \\ n_e v \end{bmatrix},$$

$$\boldsymbol{H} = \begin{bmatrix} 0 \\ 0 \\ \sigma_+ \\ 0 \\ 0 \end{bmatrix}, \boldsymbol{S} = \begin{bmatrix} 0 \\ 0 \\ 0 \\ j_z E_z + j_r E_r \\ \dot{n}_e \end{bmatrix}$$

where, ρ is the mass density, u and v are the axial and radial velocity components, respectively, n_e is the electron number density, j is the electric current density, E is the electric field, $\dot{n}_e$ is the electron production rate, t is the time, r and z are the radial and axial coordinates, respectively, and subscripts r and z mean the radial and axial components, respectively. The normal and tangential stresses are given as follows:

$$\sigma_{zz} = -p - \frac{2}{3}\mu \nabla \cdot \boldsymbol{U} + 2\mu \frac{\partial u}{\partial z} \tag{2a}$$

$$\sigma_{rr} = -p - \frac{2}{3}\mu \nabla \cdot \boldsymbol{U} + 2\mu \frac{\partial v}{\partial r} \tag{2b}$$

$$\sigma_{+} = -p - \frac{2}{3}\mu \nabla \cdot \boldsymbol{U} + 2\mu \frac{v}{r} \tag{2c}$$

$$\tau_{rz} = \tau_{zr} = \mu \left(\frac{\partial u}{\partial r} + \frac{\partial v}{\partial z} \right) \tag{2d}$$

$$\nabla \cdot \boldsymbol{U} = \frac{\partial u}{\partial z} + \frac{\partial v}{\partial r} + \frac{v}{r} \tag{2e}$$

where p is the pressure and μ is viscosity coefficient. In the present work, Sutherland's expression for viscosity coefficient is employed, which is given by

$$\mu = 22.3 \times 10^6 \frac{\tilde{T} + C}{T + C} \left(\frac{T}{\tilde{T}} \right)^{3/2} \tag{3}$$

with

$$\tilde{T} = 293.15, \quad C = 142$$

The total energy of the propellant e is given by

$$e = \frac{(1+\alpha)k_B T}{(\gamma - 1)m_a} + \frac{\alpha E_I}{m_a} + \frac{u^2 + v^2}{2} \tag{4}$$

where T is the temperature, k_B is Boltzmann's constant, γ is the ratio of specific heats, α is the degree of ionization, E_I is the energy of ionization and m_a is the mass of an atom. The equation of state for singly ionized gas is given by

$$p = (1+\alpha)\rho RT \tag{5}$$

where, R is the gas constant. The axial and radius heat fluxes are given as follows:

$$\dot{q}_z = -\lambda \frac{\partial T}{\partial z}, \quad \dot{q}_r = -\lambda \frac{\partial T}{\partial r} \tag{6}$$

where λ is the heat conductivity, which is given by

$$\lambda = \frac{15}{4}\frac{k_B}{m_a}\mu \tag{7}$$

The net production rate of the electrons $\dot{n}_e$ is written as

$$\dot{n}_e = K_1 n_a n_e - K_2 {n_e}^3 \tag{8}$$

where K_1 and K_2 are the ionization and recombination rate constants, respectively, and n_a is the neutral atom number density. In the present work, Drawin's expression for ionization rate constant for argon[7] is employed, which is given by

$$K_1 = 4\pi a_0^2 \bar{v} \left(\frac{R_\infty}{k_B T} \right)^2 \frac{\exp(-q)}{q(q+1)}$$

$$\times \left[\frac{1}{20+q} + \ln\left\{ 1.25 \left(1 + \frac{1}{q} \right) \right\} \right] \tag{9}$$

with

$$\bar{v} = \left(\frac{8k_B T}{\pi m_e} \right)^2, \quad q = E_I / k_B T$$

where m_e is the mass of an electron, a_0 is the first Bohr radius and R_∞ is Rydberg's constant. The recombination rate constant K_2 can be derived from the principle of detailed balancing and Saha equilibrium relation.

2.3 Coordinates Transformation

Numerical calculations are desirable to be made on a computational plane. In order to transform a physical plane to the computaional plane, it is necessary to generate numerical grids suitable to computations for the actual thruster geometry. The numerical grid generation is done by solving the following elliptic equations:

$$\frac{\partial^2 \xi}{\partial z^2} + \frac{\partial^2 \xi}{\partial r^2} = 0, \quad \frac{\partial^2 \eta}{\partial z^2} + \frac{\partial^2 \eta}{\partial r^2} = 0 \qquad (10)$$

The coordinates ξ and η are the transformed Cartesian coordinates. Based on the relations represented by Eq.(10) the physical plane is transformed to computational plane. Figure 2 shows the generated grids, where the typical computational plane is an upper half of the entire flow region and it is divided into 80 x 40 grids.

2.4 Boundary Conditions

The boundary conditions for gas equations are imposed as follows:

(1) Non-slip conditions are used on the cathode and anode.

(2) Symmetry conditions are employed on the nozzle axis.

(3) Outflow conditions are imposed on the exit plane of the nozzle.

(4) At the inlet, the flow is assumed to be subsonic and hence it is impossible to specify all the variables. Therefore the propellant mass flow rate, temperature and degree of ionization are specified, and $v = 0$ is set because the parallel inflow is considered. ρ is set to be equal to the value at the adjacent downstream point.

(5) The radiation cooling is considered on the cathode and anode wall. Here, considering small control volume at the wall, we get the following, as the wall temperature boundary condition:

$$S_{\rm in}\dot{q} + V_{\rm cv}\dot{j} \cdot \boldsymbol{E} = S_{\rm w}\epsilon\hat{\sigma}T_{\rm w}^4 \qquad (11)$$

where $T_{\rm w}$ is the wall temperature, ϵ is the emissivity of the wall, $\hat{\sigma}$ is Stefan-Boltzmann's constant, $S_{\rm in}$ is the area of the control volume for the influx of the heat, $S_{\rm w}$ is the wall area of the control volume and $V_{\rm cv}$ is the volume of the control volume. Figure 3 shows above boundary. The first term represents the influx of the energy, the second term denotes the Joule heating in the control volume and the right hand side represents the efflux of the energy. Because $V_{\rm cv}$ is very small, the second term is neglected ordinarily. But it is clarified from our calculation that $\dot{j} \cdot \boldsymbol{E}$ is very large, so the second term must be included.

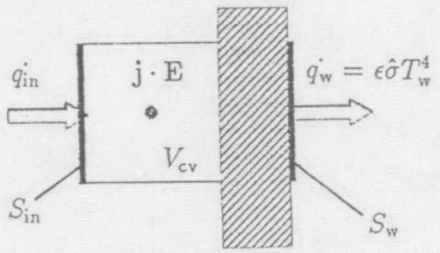

Fig.3 Wall boundary.

3. Governing Equations for Electric Field

The arcjet thruster considered here is a low power thruster, so that discharge currents are relatively small. Hence, hall currents and ion slip may be neglected. According to the previous result[5] , Lorentz force caused by the interaction of the electric current density and induced magnetic flux, $\dot{j} \times \boldsymbol{B}$ is very small, and the Lorentz force term is excluded from the present momentum equation. The electric field equation is represented by Ohm's law and Maxwell equation, and written in steady state form. These are given by the followings:

$$\dot{j} = \tilde{\sigma}\boldsymbol{E} \qquad (12a)$$

$$\nabla \cdot \dot{j} = 0 \qquad (12b)$$

$$\nabla \times \boldsymbol{E} = 0 \qquad (12c)$$

where $\tilde{\sigma}$ is the electrical conductivity which is given by Spitzer's free path theory[8]:

$$\tilde{\sigma} = \frac{3.05 \times 10^{-12} n_{\rm e}}{\sqrt{T}\sum_j n_j Q_{ej}} \ \text{mho/m} \qquad (13)$$

where n_j is the number density of species j and Q_{ej} is the collision cross section for electron-species j encounters which is given by, for argon :

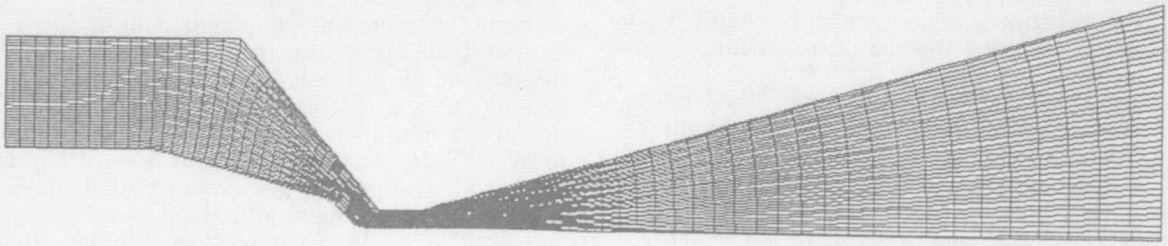

Fig.2 Grid generation.

$$Q_{ea} = (0.39 - 0.551 \times 10^{-4}T + 0.595 \times 10^{-8}T^2) \times 10^{-20} \quad m^2 \text{ for } T < 10{,}000 \text{ K} \tag{14a}$$

$$Q_{ea} = (-0.35 + 0.551 \times 10^{-4}T) \times 10^{-20} \quad m^2 \text{ for } T > 10{,}000 \text{ K} \tag{14b}$$

$$Q_{ei} = \frac{5.85 \times ln\Lambda}{T^2} \times 10^2 \ m^2 \tag{14c}$$

$$Q_{ee} = 0.707 Q_{ei} \ m^2 \tag{14d}$$

with

$$\Lambda = \frac{1.24 \times 10^7 T^{\frac{3}{2}}}{\sqrt{n_e}} \quad (n_e : 1/m^3, \quad T : K)$$

And electric potential is written as follows:

$$E_x = -\frac{\partial \phi}{\partial x}, \quad E_y = -\frac{\partial \phi}{\partial y} \tag{15}$$

Then the following electric potential equation is derived from the above equations:

$$\tilde{\sigma}\left(\frac{\partial^2 \phi}{\partial x^2} + \frac{\partial^2 \phi}{\partial y^2}\right) + \frac{\partial \tilde{\sigma}}{\partial x}\frac{\partial \phi}{\partial x} + \left(\frac{\partial \tilde{\sigma}}{\partial y} + \frac{\tilde{\sigma}}{y}\right)\frac{\partial \phi}{\partial y} = 0 \tag{16}$$

This partial differential equation is transformed to the computational plane(ξ ,η) and then rewritten to a difference equation with second order accuracy in space, and solved numerically using Jacobi's method.

Wall boundary conditions are given by

$$\phi = \begin{cases} V & \text{on the anode} \\ 0 & \text{on the cathode} \end{cases} \tag{17}$$

$$\frac{\partial \phi}{\partial r} = 0 \text{ on the center line.} \tag{18}$$

The electric voltage V is given by electrical conductivity and input power.

4. Numerical Procedure

Firstly, the numerical calculation for arc-off is performed, using the quasi one-dimensional Euler equation solutions as initial conditions. Thus obtained arc-off solutions are utilized as initial conditions for arc-on computations. The computations are performed with a hybrid scheme that consists of following sequence of operation:

(1) Electrical conductivities are determined based on known temperatures and electron number densities. At the first time step, the degree of ionization 10^{-5} is given at all the grid points except the inlet.

(2) Based on known electrical conductivities, the solutions of the electric field are obtained.

(3) A set of the propellant gas flow equations are transformed to the new coordinates system (ξ, η) and then numerically solved by using the TVD-MacCormack scheme [9] based on known electric properties. At each time step, the time increment δt is determined so as to satisfy both the CFL and stability conditions to solve the equation including ionization-recombination reaction.

(4) Steps (1) to (3) are repeated until the steady state solutions are attained as asymptotic solutions to the unsteady equation for large time.

5. Results and Discussion

As described above, the temperature, radial velocity, degree of ionization and mass flow rate are specified at the inlet (cf. Table 1). Input power is set to 140 W. On the view of a low power thruster with 1 kw, the present power seems far from the actual one. However, the computations for larger power than 140 W did not successful due to computational instability. There was large difficulty even in the calculation for 140 W. Initially the solution for 5 W was obtained and then this solution is used as the initial conditions for slightly large power. Thus slow startup procedure from very low power solutions was needed to avoid instability. On the other hand, the calculations for constant temperature as wall condition were tried for a 1 kw thruster and showed successful results though they are not shown in this paper.

Table 1: Inlet conditions

Temperature (K)	Mass flow rate (g/s)	Degree of ionization	Radial velocity (m/s)
300	0.11	0.0	0.0

Figure 4 shows the velocity vectors for arc-off and arc-on. From this figure, it is seen that the flow in the case of arc-on is remarkably accelerated downstream of the constrictor and that the exhaust velocity is much larger than that in the case of arc-off. But arc-on boundary layer is thicker than arc-off. Because mass flow rate is constant, density in the case of arc-on become smaller than that in the case of arc-off, as the velocity becomes larger. So the Reynolds number in the case of arc-on at the expansion part is smaller than that in the case of arc-off. For this reason, the boundary layer becomes thick in the arc-on case.

Figure 5 represents the field contour lines of temperature, pressure, propellant gas density, electron number density. The pressure and propellant gas density are drawn on logarithmic scale. In Table 2 are given the maximum and minimum values. Figure 5(a) is the contour lines of temperature. The propellant gas enters the thruster at a temperature of 300K and then temperature is increased by Joule heating. But on the wall, the

gas is cooled by wall radiation. Therefore maximum temperature is not attained on the anode surface, and it exists far from the wall. The maximum temperature point is upstream of the constrictor, which is caused by large concentration of arc current (cf. Fig.6). Figure 6 shows the contour lines of the arc current density. The maximum temperature, the maximum anode temperature and the maximum cathode temperature are also shown in Fig.5(a). The maximum temperature is 3000 K, the maximum anode temperature is 1994 K and the maximum cathode temperature is 1440 K. As shown in Fig.5(a), there is the high temperature ring. The velocity in the ring is much larger than near wall. The total energy is non-uniform in the radial direction. For this reason, in the divergent part, the velocity of the stream from the ring is more remarkably accelerated than that near the wall. Therefore, in the divergent part, the velocity of the central flow is smaller than that of the flow around. But as going to downstream, such velocity distribution disappears and the velocity of the central flow becomes larger than that of the flow around.

The thruster performance for $\dot{m} = 0.11$ g/s is as follows:

Thrust = 0.129 N, Specific Impulse = 120 s.

The efficiency is given by

$$\eta = \frac{(K.E.)_{\text{exit}}}{H_{\text{inlet}} + VJ}$$

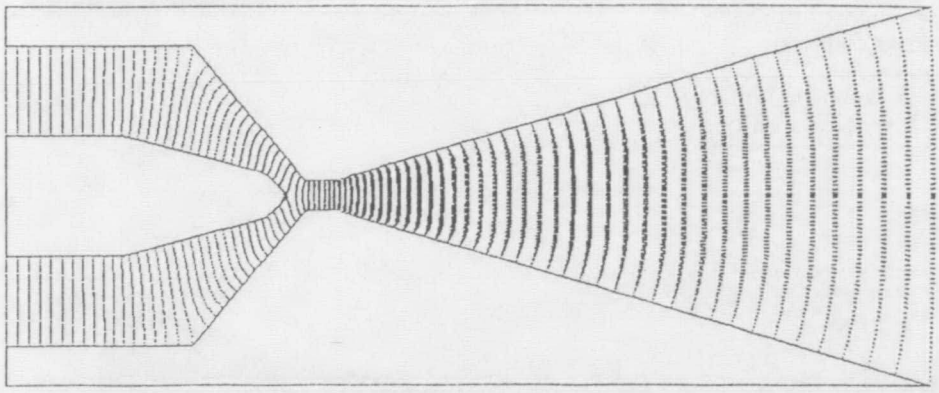

(a) arc-off

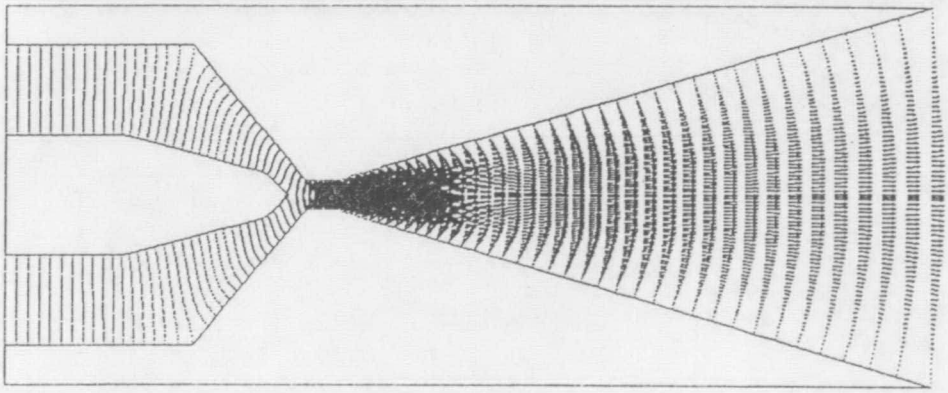

(b) arc-on

Fig.4 Velocity vectors (arc-off and on).

Table 2: Maximum and minimum value in Fig.5

	Temperature (K)	Pressure (N/m^2)	Density (kg/m^3)	Degree of ionization	Current density (A/m^2)
Maximum	3004.7	1.8251×10^{3}	0.6048	4.7585×10^{-5}	8.388×10^{5}
Minimum	193.8	0.155	3.2196×10^{-4}	7.25×10^{-78}	0.0

where $(K.E.)_{exit}$ is the kinetic energy at the nozzle exit, H_{inlet} is the total enthalpy at the inlet and VJ is the input power. In the present calculation, $(K.E)_{exit}$=81.1 W, H_{inlet} =10.2 W and VJ=140 W, and hence we have η =53.9 %.

6. Concluding Remarks

In the present study, the numerical simulation code for a low power arcjet thruster was developed. This code includes nonequilibrium ionization-recombination, viscous effect and heat transfer on the wall, and treats a subsonic inlet flow. The computation is performed on the numerical grids so as to fit the actual thruster geometry. The computations using the radiation cooling condition as wall condition are successful only for a very low power. Computational instability occurred in larger power than the present input power. Nevertheless the interesting results were obtained. They are summarized as follows:

(1) Boundary layer is very thick downstream of the constrictor due to low Reynolds number.

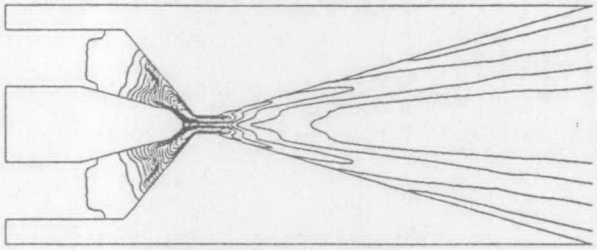

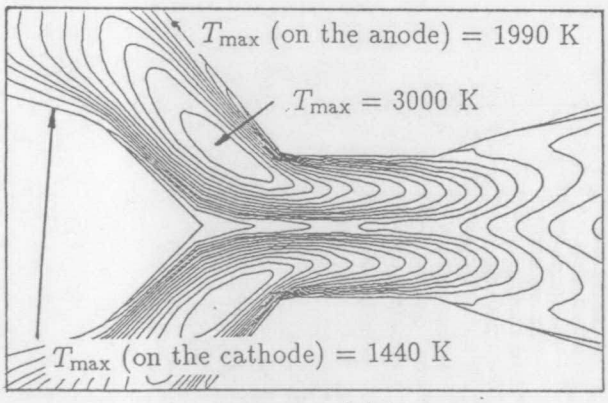

near constrictor

Fig.5(a) Temperature.

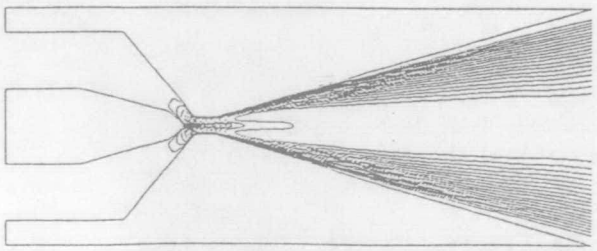

Fig.5(b) Equi-velocity lines.

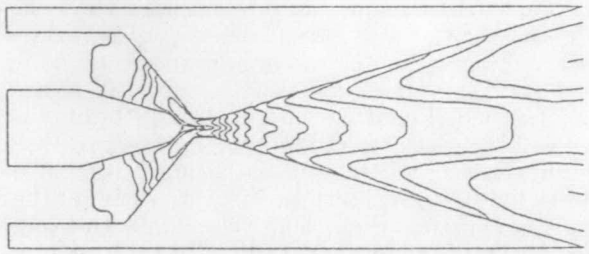

Fig.5(c) Density.

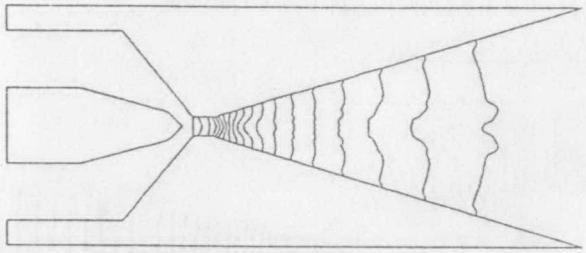

Fig.5(d) Pressure.

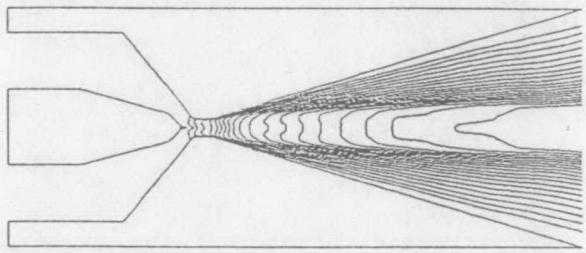

Fig.5(e) Mach number.

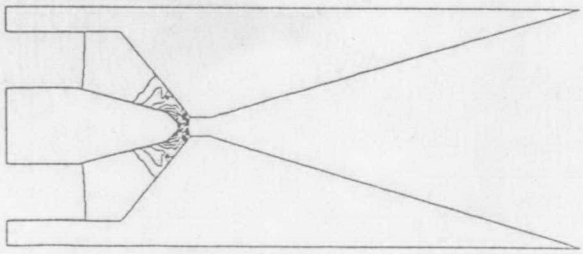

Fig.6 Current density.

(2) Degree of ionization is less than 10^{-5} in the whole flow filed and hence the effect of the charged species on the flow is negligible.

(3) The maximum temperature is found in the flow in the convergent part of the nozzle. The maximum degree of ionization and the maximum electrical conductivity are observed slightly upstream of the maximum temperature point.

References

(1) T. Ao and T. Fujiwara, Numerical and Experimental Study of an MPD thruster, In Proceedings of the 17th International Electric Propulsion Conference, Tokyo, 1984, pp.55-64.

(2) H. Yamada and T. Fujiwara, Computational Fluid Dynamics Study of an MPD Thruster, Memoirs of Faculty of Engineering, Nagoya University, Vol.38 (1986), pp.261-278.

(3) J. M. G. Chanty and M. Martinez-Sanchez, Two-dimensional Numerical Simulation of MPD Flows, AIAA-87-1090 (19th International Electric Propulsion conference), (1987).

(4) P. C. Sleziona, M. Auweter-Kurtz and H. O. Schrade, Numerical Codes for Cylindrical MPD Thrusters, In Proceedings of th 20th International Electric Propulsion Conference, Garmisch-Partenkirchen, 1988, pp.224-234.

(5) M. Nishida, K. Kaita and K. Tanaka, Numerical Study of the Flow Field in a DC Arcjet Thruster, In Proceedings of the 20th International Electric Propulsion Conference, Garmisch-Partenkirchen, 1988, pp.591-597.

(6) K. Tanaka, K. Tsuchiya, K. Kaita and M. Nishida, Experimental Investigation on the Characteristics of a Low Power DC Arcjet Thruster, In Proceedings of the 20th International Electric Propulsion Conference, Garmisch-Partenkirchen, 1988, pp.620-626.

(7) H. W. Drawin, EUR-CEA-FC-383, Association Euratom C.E.A., Fortenay-aux-Roses, France, (1967).

(8) A. B. Cambel, Plasma Physics and Magnetofluid-mechanics, McGraw-Hill , New-York , pp.152-191 (1963).

(9) S. F. Davis, A Simplified TVD Finite Difference Scheme via Artificial Viscosity, ICASE Report, No.84-20, June (1984).